Suction Caisson Installation in Sand with Isotropic Permeability Varying with Depth

Ouahid Harireche, Moura Mehravar, Amir M. Alani

Department of Civil Engineering.MedwaySchool of Engineering.University of Greenwich, Kent, ME4 4TB, UK.

Corresponding Author

Ouahid Harireche.
University of Greenwich at Medway.
Central Avenue
Chatham Maritime
Kent ME4 4TB
Telephone: +44 (0)1634 883787
Fax: +44 (0)1634 883153
E-mail: o.harireche@gre.ac.uk

Abstract

Suction-induced seepage is pivotal to the installation of caisson foundations in sand. Indeed, the upward pore water flow on the inner side of the caisson wall causes a release of a fraction of soil resistance due to the reduction of the lateral effective stress. A safe caisson installation requires a reliable prediction of soil conditions, especially soil resistance and critical suction for piping. These soil conditions must be predicted for the whole installation process.

In this paper, we examine the effect of the assumed permeability profile, as a function of depth below the mudline, on such prediction. This study is motivated by the fact that marine sediments generally exhibit a permeability that decreases with depth because of consolidation under gravity. Hence, the question is whether conventional theories based on a constant permeability lead to a conservative prediction of soil conditions. Our conclusion is affirmative only regarding piping condition. As for soil resistance, a prediction based on the assumption of a constant permeability is non conservative. This is due to an overestimated reduction in effective stresses under suction-induced seepage.

Keywords

Caisson foundation; Installation in sand; Normalised geometry; Piping condition; Permeability varying with depth.

1. Introduction

A Suction caisson consists of a thin-walled upturned ‘bucket’ of cylindrical shape made from steel. This type of foundation has proven to be efficient and versatile as a support for offshore structures and appears to be a very attractive option for future use in offshore wind turbines [1, 2].

The installation procedure starts by lowering the caisson into the seabed where an initial penetration is achieved under caisson self-weight. Seabed material surrounding the caisson wall above the caisson tip forms a natural seal which is vital to the initial installation stage. Water trapped inside the caisson cavity is then pumped out, which imposes a suction that results into a pressure differential on the caisson lid. At mudline level, inside the caisson cavity, the imposed suction, which will be assumed uniformly distributed in this work, induces seepage around the caisson wall. For a caisson installation in sand, seepage causes an overall reduction in soil resistance and facilitates caisson penetration. It is often recognised that the downward force produced by suction wouldn’t overcome soil resistance for installation in sand if no soil loosening is achieved due to the induced seepage [3-8]. Most design procedures of caisson installation in sand take into account the role of porewater seepage induced by suction [9-12]. The role of suction during caisson installation in sand has also been considered in centrifuge model testing [13] and finite element simulations [14]. The existence of low permeability silt layers has been considered by Tran et al., [15].

During caisson installation in sand, suction must be controlled to avoid the formation of piping channels which would prevent further penetration and may cause the installation procedure to fail [16]. The development of design procedures with effective suction control requires a good understanding of soil conditions and seepage around the caisson wall. Effects of seepage on soil conditions, such as piping and soil resistance, must be predicted for the whole installation process to ensure that changes in suction remain within the safety limits. Using a finite difference procedure applied to the normalised seepage problem of caisson installation in sand, Harireche et al., [17] described soil conditions and derived criteria for suction control during caisson installation in sand. The numerical procedure they proposed takes into account the actual variation in excess pressure gradient over the installation depth.

In the present paper, the numerical procedure proposed by Harireche et al., [17] is extended to take into account a seabed permeability that decreases with depth. Bryan et al. [18] reported field data for marine sediments in the Gulf of Mexico. Their measurements show that soil permeability generally decreases with an increasing depth. Bennett et al. [19] have also performed in-situ measurements of porosity and permeability of selected carbonate sediments and their reported data provides further evidence for soil permeability varying with depth. The present study is motivated by the need to assess whether a homogeneous seabed model is a conservative assumption for caisson installation design.

2. Normalised seepage problem and permeability profiles

We consider a caisson of radius *R*, height *L* and we denote *h* the depth of caisson penetration into the seabed. The soil consists of sand with permeability *k* decreasing with the depth *z* below the mudline. A normalised problem geometry where all dimensions are scaled with respect to the caisson radius is adopted. Figure 1 shows a vertical section through the meridian plane of the system caisson-soil where a cylindrical system of coordinates r^* and z^* is used. The hydrostatic porewater pressure that exists in the soil before caisson installation is denoted p_0 and has a magnitude at depth *z*, $p_0 = p_{at} + \gamma_w h_w + \gamma_w z$, where p_{at} is the atmospheric pressure, γ_w the unit weight of water and h_w the water height above the mudline. During caisson installation the imposed suction induces a deviation of porewater pressure from the hydrostatic value, which will be referred to as excess porewater pressure and will be denoted *p*. The suction magnitude, $\bar{s}$ imposed over the radial distance OC^- (Fig. 1) is expected to increase during installation. Indeed, as the caisson is pushed into the seabed, suction must be increased to overcome the increasing soil resistance. On the mudline boundary C^+F outside the caisson, and on the boundaries FH and BH sufficiently far from the zone of significant pressure disturbance, the initial hydrostatic pressure p_0 is not affected.

Figure 1

In order to describe the variation of permeability with depth, the following expression is adopted:

$$\bar{k} \equiv \frac{k(z^*)}{k_0} = (1-\beta)\,e^{-\alpha z^*} + \beta \qquad (1)$$

In this equation, $k \equiv K / n\gamma_w$, where K is the absolute permeability and n denotes the porosity. The coefficient k_0 denotes the permeability at the seabed surface, $z^*=z/R$ the normalised depth and α, β are two constants such that:

$$\alpha > 0\,; \qquad \beta = \frac{k_\infty}{k_0}, \qquad 0 \le \beta \le 1 \qquad (2)$$

Note that for $\beta = 1$, the case of a homogeneous seabed with a constant permeability k_0 is recovered. A value $\beta = 0$ corresponds to an impervious condition at large depth, i.e., $k_\infty = 0$.

In order to identify the constants α and β for a given seabed profile, k_∞, k_0 and $\bar{k}_1 = \bar{k}(z_1^*)$, for a given normalised depth z_1^*, must be specified. The coefficient β can be calculated using the second relation (2) and α is given by:

$$\alpha = \frac{1}{z_1^*} Ln\left(\frac{1-\beta}{\bar{k}_1 - \beta}\right) \qquad (3)$$

Figure 2 shows different permeability profiles and the corresponding values of the parameters α and β. Three cases have been selected, which will be investigated in the following sections. Case A corresponds to a homogeneous seabed profile with constant permeability. In case B, the permeability decreases with depth almost linearly. A value $\bar{k} = 0.75$ is achieved at depth $z = R$ using $\beta = 0$ and $\alpha = 0.288$. In case C, permeability has a non-linear profile and decreases with depth at a much higher rate compared to case B. At depth $z = R$, a value $\bar{k} = 0.30$ is achieved using $\beta = 0$ and $\alpha = 1.204$. Note that in both cases B and C, the soil is assumed to become impervious at large depth.

Figure 2

The porewater seepage is assumed to obey Laplace's equation:

$$div(-k\nabla p) = 0 \tag{4}$$

Where ∇p denotes the excess porewater pressure gradient and,

$div \equiv (1/r)\partial/\partial r + (1/r)\partial/\partial\theta + \partial/\partial z$.

Denoting $k' \equiv dk/dz$, equation (4) can be developed in axisymmetric conditions ($\partial/\partial\theta = 0$) to give:

$$\frac{\partial^2 p}{\partial r^2} + \frac{1}{r}\frac{\partial p}{\partial r} + \frac{\partial^2 p}{\partial z^2} + \frac{k'}{k}\frac{\partial p}{\partial z} = 0 \tag{5}$$

In order to draw conclusions that are not affected by the problem dimensions, we adopt the following scaling of the main problem variables:

$$p^* = \frac{p}{s},\ h^* = \frac{h}{R},\quad r^* = \frac{r}{R}\quad (0 \le \mathrm{r}^* \le 1 \text{ on OC and } 1 \le \mathrm{r}^* < \infty \text{ on CF}) \tag{6}$$

The scaled porewater pressure p^* satisfies the dimensionless equation:

$$\frac{\partial^2 p^*}{\partial r^{*2}} + \frac{1}{r^*}\frac{\partial p^*}{\partial r^*} + \frac{\partial^2 p^*}{\partial z^{*2}} + f^*(z^*)\frac{\partial p}{\partial z^*} = 0 \qquad (7)$$

Where:

$$f^*(z^*) \equiv \frac{-\alpha(1-\beta)}{1-\beta+\beta e^{\alpha z^*}} \qquad (8)$$

As the caisson penetrates into the seabed, radial porewater flow across the caisson wall is prevented, which is described by the boundary condition on CD: $\partial p / \partial r = 0$ and due to symmetry, this condition must also be satisfied on the z-axis (i.e., for $r = 0$). As shown in Figure 1, the soil domain is divided into four regions. Region (Ω_1) represents soil inside the caisson, (Ω_2) is the region occupied by soil which passes inside the caisson after further penetration and regions (Ω_3) and (Ω_4) are the complementary soil regions outside the caisson, surrounding (Ω_2) and (Ω_1) respectively. In addition to equation (7), the scaled excess porewater pressure p^* must satisfy the boundary conditions:

$$p^* = -1 \text{ on } OC^-, \quad p^* = 0 \text{ on } C^+F, FH, BH \text{ and } \quad \frac{\partial p^*}{\partial r^*} = 0 \text{ on CD and OB} \qquad (9)$$

3. Finite difference solution of the normalised problem

A simple finite difference scheme is used to solve the model problem presented in the previous section. The coordinates r^* and z^* are discretised into constant increments Δr^* and Δz^* and the following approximations are adopted:

$$\left.\frac{\partial p^*}{\partial r^*}\right|_{i,j} \cong \frac{p^*_{i,j+1} - p^*_{i,j}}{\Delta r^*}$$

$$\left.\frac{\partial p^*}{\partial z^*}\right|_{i,j} \cong \frac{p^*_{i+1,j} - p^*_{i,j}}{\Delta z^*} \tag{10}$$

$$\left.\frac{\partial^2 p^*}{\partial r^{*2}}\right|_{i,j} \cong \frac{p^*_{i,j+1} - 2p^*_{i,j} + p^*_{i,j-1}}{\Delta r^{*2}}$$

$$\left.\frac{\partial^2 p^*}{\partial z^{*2}}\right|_{i,j} \cong \frac{p^*_{i+1,j} - 2p^*_{i,j} + p^*_{i-1,j}}{\Delta z^{*2}}$$

Where $i=1$ on the mudline (OF) and $j=1$ on the vertical axis (OB).

Using the finite difference scheme above, equation (7) is approximated by:

$$\begin{aligned}&\left[2\left(\frac{1}{\Delta r^{*2}} + \frac{1}{\Delta z^{*2}}\right) + \frac{1}{r^*\Delta r^*} + \frac{f_i^*}{\Delta z^*}\right] p^*_{i,j} - \\ &\qquad \left(\frac{1}{\Delta r^{*2}} + \frac{1}{r^*\Delta r^*}\right) p^*_{i,j+1} - \frac{1}{\Delta r^{*2}}\, p^*_{i,j-1} - \left(\frac{1}{\Delta z^{*2}} + \frac{f_i^*}{\Delta z^*}\right) p^*_{i+1,j} - \frac{1}{\Delta z^{*2}}\, p^*_{i-1,j} = 0\end{aligned} \tag{11}$$

Where $f_i^* \equiv f^*((i-1)\times\Delta z^*)$ and $f^*(z^*)$ is defined by (8).

On the z-axis, the condition

$$\lim_{r^*\to 0} \frac{1}{r^*}\frac{\partial p^*}{\partial r^*} = \frac{\partial^2 p^*}{\partial r^{*2}} \tag{12}$$

leads to the approximation form:

$$\left.\frac{1}{r^*}\frac{\partial p^*}{\partial r^*}\right|_{i,j} \cong \frac{2(p^*_{i,j+1} - p^*_{i,j})}{\Delta r^{*2}} \tag{13}$$

An important aspect of the present numerical procedure is to enforce the continuity of excess pore water pressure p^* at point D (Fig.1).

$$p^*(D)\Big|_{\Omega_1} = p^*(D)\Big|_{\Omega 4} \qquad (14)$$

Applying equation (11) to point D, separately in domains (Ω_1) and (Ω_4), taking into account condition (14) and the third boundary condition (9), leads to the approximation below:

$$2\left(\frac{1}{\Delta r^{*2}}+\frac{2}{\Delta z^{*2}}+\frac{f^*(D)}{\Delta z^*}\right)p_D^* - \frac{1}{\Delta r^{*2}}\,p_{DL}^* - \frac{1}{\Delta r^{*2}}\,p_{DR}^* - \frac{1}{\Delta z^{*2}}\,p_{I^-}^* - \frac{1}{\Delta z^{*2}}\,p_{I^+}^* - 2\left(\frac{1}{\Delta z^{*2}}+\frac{f^*(D)}{\Delta z^*}\right)p_J^* = 0 \qquad (15)$$

Where points D, D_L, D_R, I^-, I^+ and J are shown in Figure 1.

The finite difference approximations presented in this section have been implemented in a computer program which has been used to analyse seepage around a suction caisson as installation progresses in sand with a permeabilitydecreasing with depth. This analysis is performed to study the effects of suction induced seepage on soil resistance for the different permeability profiles described in section 2. Critical conditions for piping are also considered within this extended context of permeability varying with depth. These aspects are reported and discussed in the following sections.

4. Soil resistance to caisson penetration

Water seepage caused by suction produces a hydraulic gradient which, on both faces of the caisson wall, varies with depth. Figures 3a, 3c and 3e show the contours of normalised excess pore pressure p^* for values of the scaled penetration depth h^* = 0.2 (typical of self-weight penetration), 1 and 2. These figures correspond to a homogeneous seabed with constant permeability. For comparison, figures 3b, 3d and 3f show similar contours for a seabed profile that corresponds to case C described in section 2. These figures show clearly that the pressure distribution is affected by the permeability profile, although this effect is not noticeable at the early stage where the installation depth is typical of self-weight penetration (Fig. 3b).

<u>Figure 3</u>

Figure 4 shows the vertical component of the normalised pressure gradient $g^* \equiv \partial p^* / \partial z^*$ on both sides of the caisson wall as a function of scaled depth z^* for the three permeability profiles (cases A, B and C). Values of scaled penetration depth h^* = 0.2, 1 and 2 have been considered.

It can be seen that the pressure gradient on each side of the caisson wall is higher at the early stages of the installation process. Maximum values of the gradient occur at the caisson tip. For the homogeneous seabed profile with constant permeability (case A), the gradient distribution over the caisson embedment tends to become uniform over a significant depth as the installation proceeds. A gradient of higher magnitude tends to localise around the caisson tip. For seabed profiles where the permeability decreases with depth (cases B and C), such a uniformity is less pronounced, especially for the gradient on the inner side. By comparing the normalised gradients for the three different cases A, B and C, on both sides of the caisson wall, it can be observed that the effect of permeability profile becomes more important as the penetration depth increases. For the normalised gradient on the outer side, the difference in gradient magnitude for the three permeability profiles is not significant at shallow depths. However, such a difference increases with depth, which is likely to affect soil resistance through the increase in effective stress and this will be more noticeable at later stages during the caisson installation process. On the inner side of the caisson wall, the normalised gradient magnitude is affected in a different way. Up to a scaled depth which can be estimated to 3/4 of the scaled penetration depth, the normalised gradient magnitude is lower for a higher rate of variability in the permeability profile. Below such depth, the opposite trend is observed. This behaviour suggests that soil is less prone to piping for a permeability that has a higher variability profile. In terms of soil resistance to caisson penetration, it can be anticipated that a higher variability profile is likely to correspond to less reduction in soil resistance due to seepage. If this is the case, then we would conclude that soil resistance estimations based on a constant permeability assumption are not conservative.

<u>Figure 4</u>

These effects are now studied in more detail in order to withdraw final conclusions regarding soil resistance against caisson penetration and critical condition for piping.

4.1 Lateral frictional resistance on caisson wall

In the absence of seepage, the lateral effective pressure on the caisson wall has the expression:

$$\sigma_h^{'} = K(\gamma' z + \tilde{\sigma}) \qquad (16)$$

Where K is a lateral earth pressure coefficient. The vertical effective stress near the caisson wall is enhanced by the magnitude $\tilde{\sigma}$ due to the effect of shear resistance that develops on the interface soil-caisson. Under seepage conditions produced by an applied suction, the lateral effective pressure acting on the caisson wall at depth *z*, inside and outside the caisson is respectively expressed as follows:

$$\sigma'_{hi}(R,z) = K\left(\gamma' z - \int_0^z g_i(R,\zeta)d\zeta + \tilde{\sigma}_i(R,z)\right) \tag{17}$$

$$\sigma'_{ho}(R,z) = K\left(\gamma' z - \int_0^z g_o(R,\zeta)d\zeta + \tilde{\sigma}_o(R,z)\right) \tag{18}$$

Where $g_i(R,\zeta)$ and $g_o(R,\zeta)$ denote the vertical component of the pressure gradient on the inner and the outer sides of the caisson wall respectively. Assuming that the enhanced effective stresses $\tilde{\sigma}_i$ and $\tilde{\sigma}_o$ are not affected by seepage conditions, the reduction at depth *z* in the lateral pressure acting on the caisson wall caused by seepage is given by:

$$\Delta\sigma'_h(R,z) = K\left(\int_0^z g_i(R,\zeta)d\zeta + \int_0^z g_o(R,\zeta)d\zeta\right) \tag{19}$$

The pressure gradients can be expressed as follows:

$$g_o = \frac{\bar{s}}{R} g_o^*; \quad g_i = \frac{\bar{s}}{R} g_i^* \tag{20}$$

Where $g_0^* \equiv \partial p^* / \partial z^*$ is the normalised pressure gradient in domains (Ω_4), (Ω_3) and $g_i^* \equiv \partial p^* / \partial z^*$ denotes the same quantity when evaluated in domains (Ω_1) and (Ω_2).Hence, expression (19) can be rewritten under the following form:

$$\frac{\Delta\sigma'_h(R,z)}{K\bar{s}} = L_i^*(z^*) + L_o^*(z^*) \tag{21}$$

Where, as can be seen from Figure 4:

$$L_i^*(z^*) \equiv \int_0^{z^*} g_i^*(1,\zeta^*)d\zeta^* > 0\,,\; L_o^*(z^*) \equiv \int_0^{z^*} g_o^*(1,\zeta^*)d\zeta^* < 0 \;\text{ and }\; \left|L_i^*(z^*)\right| > \left|L_o^*(z^*)\right| \tag{22}$$

Using a numerical calculation of the integrals in (22) on the normalised finite difference mesh, we obtain the scaled reduction of the lateral effective stress expressed in (21) as a function of the normalised depth z^*, which is shown in Figure 5. It can be observed that such a reduction increases with depth and is clearly affected by the permeability profile. A higher rate of variability in the permeability corresponds to a lower reduction in the lateral effective stress. Although this effect is quite limited at shallow penetration depths (Fig. 5a), it is clearly more pronounced at larger penetration depths (Figs. 5b-c). This shows clearly that the assumption of a homogeneous seabed is not in favour of a conservative estimation of soil resistance to caisson penetration as it overestimates the effect of seepage on the reduction of the lateral effective stress.

Figure 5

As a consequence, seepage causes the frictional resisting force acting on the caisson wall to decrease by a magnitude ΔF_s given as a function of the scaled penetration depth h^* by the expression:

$$\frac{\Delta F_s}{2\pi R^2 K\overline{s}} = \int_0^{h^*} \left[L_i^*(z^*) + L_o^*(z^*) \right] dz^* \tag{23}$$

4.2 Tip resistance

Seepage also causes the vertical effective stress at the caisson tip to decrease, thereby leading tofurther reduction in the total resisting force. The resisting force at the caisson tip can be expressed under the form:

$$F_t = 2\pi R N_q \int_{R_i}^{R_e} \sigma_v^{'} dr \tag{24}$$

Where N_q is a bearing capacity factor and $\sigma_v^{'}$ the vertical effective stress at the caisson tip, which is assumed to vary linearly from $\sigma_{vi}^{'}$ inside the caisson (radius R_i) to $\sigma_{vo}^{'}$ outside (radius R_o), and these stresses have the expressions:

$$\sigma_{vi}^{'}(R,h) = \gamma^{'} h - \int_0^h g_i(R,\zeta) d\zeta + \tilde{\sigma}_i(R,h) \tag{25}$$

$$\sigma_{vo}^{'}(R,h) = \gamma^{'} h - \int_0^h g_o(R,\zeta) d\zeta + \tilde{\sigma}_o(R,h) \tag{26}$$

Assuming that seepage does not affect the enhanced vertical stress, the resisting force at the caisson tip decreases by the magnitude ΔF_t such that:

$$\frac{\Delta F_t}{2\pi R t N_q \overline{s}} = \frac{1}{2}\left(L_i^*(h^*) + L_o^*(h^*) \right) \tag{27}$$

where functions $L_i^*(z^*)$ and $L_o^*(z^*)$ are defined by expressions (22).

Figure 6 shows the expression $(L_i^*(h^*) + L_o^*(h^*))$ as a function of penetration depth (h^*) for the three permeability profiles considered in this study. Figure 6 and expression (27) show clearly that the reduction in the magnitude of tip resistance is maximum when permeability is assumed constant (case A). Hence, constant permeability profile is not a conservative assumption when estimating tip resistance to caisson penetration.

5. Critical suction for piping condition

During caisson installation in sand, suction magnitude must be controlled to avoid the formation of piping channels around the caisson wall, which may cause the installation procedure to fail [16].

At a generic material point of normalised coordinates r^*, z^* within the soil in contact with the inner side of the caisson wall, piping takes place when the vertical effective stress becomes zero. This is expressed by the equation:

$$\sigma_v' = \gamma' z - \int_0^z g_i(R,\zeta)d\zeta = 0 \tag{28}$$

Hence, the suction magnitude that causes such condition is given by:

$$\frac{s_{cr}}{\gamma' R} = \frac{z^*}{L_i^*(1,z^*)} \tag{29}$$

Where $L_i^*(1,z^*) \equiv \int_0^{z^*} g_i^*(1,\zeta^*)d\zeta^*$.

Note that expression (29) is similar to the one derived by Houlsby and Byrne [10] under the form $s_{cr}/(\gamma' R) = h^*/(1-a)$ where a is the magnitude of the normalised pressure at the caisson tip on the inner side; i.e. $a \equiv -p^*(h^*)$.

The present criterion extends the expression proposed by Houlsby and Byrne [10], taking into account the actual variation of the pressure gradient as a function of depth. At the caisson tip, it has the expression: $s_{cr}/(\gamma' R) = \dfrac{h^*}{L^*{}_i(1,h^*)}$. Note that, in addition to the variable pressure gradient, the present criterion also takes into consideration a permeability varying with depth, which is implicitly accounted for in the expression of $L^*{}_i(1,h^*)$.

Figure 7 shows the variation of the normalised magnitude of critical suction, $s_{cr}/(\gamma' R)$ as a function of depth at three different stages of the installation process where the scaled penetration depth is 0.2, 1 and 2. The three permeability profiles have been considered at each stage for comparison. It can be observed that the assumption of a homogeneous soil (case A) leads to the estimation of a minimum critical suction. Hence, as far as the condition for piping is concerned, such an assumption is conservative. It can be observed from Figure 7 that, while the effect of the variability with depth of permeability is less pronounced around the caisson tip, it becomes very significant at shallow depth.

Figure 7

6. Conclusion

In this study we have considered the effect of a permeability varying with depth on the prediction of soil resistance to caisson penetration and critical suction for piping condition.

Three permeability profiles have been considered, namely: constant permeability, permeability slowly varying with depth (α = 0.288), permeability with a high variability with depth (α = 1.204). These profiles have been motivated by the fact that marine sediments are expected to exhibit a permeability that decreases with depth at a rate that must also be taken into consideration as it may vary from one type of soil to another. The effect of suction induced seepage on soil resistance to caisson penetration has been investigated using the normalised solution of seepage around the caisson wall. It has been observed that a constant permeability profile leads to an under-estimation of soil resistance to caisson penetration. This highlights the importance of taking into account a permeability profile with certain variability with depth for a more accurate prediction of the required suction throughout the installation process. The investigation of piping on the inner side of the caisson wall revealed that the constant permeability assumption under-estimates the critical suction for piping. As far as the formation of piping channels is concerned, the assumption of homogeneous seabed with constant permeability is conservative. However, taking into account the actual variability with depth of the permeability may lead to a more accurate estimation of the critical suction with significantly less restriction on the safe suction profile throughout the installation process.

Acknowledgement

Funding of a PhD scholarship by the University of Greenwich to support the second author is gratefully acknowledged.

References

1. Byrne, B. W., Houlsby, G. T., Martin, C., Fish, P., 2002. Suction caisson foundations for offshore wind turbines. Wind Engineering, 26(3), 145-155.

2. Byrne, B.W., Houlsby, G.T., 2003. Foundations for offshore wind turbines. Philosophical Transactions of the Royal Society of London, series A, 361, 2909-2930.

3. Erbrich, C.T.,Tjelta, T.I., 1999. Installation of bucket foundations and suction caissons in sand: geotechnical performance. Offshore Technology Conference, Houston, TX, Paper OTC 10990, 11pp.

4. Senders, M. and Randolph, M. F., 2009. CPT-Based Method for the Installation of Suction Caissons in Sand. Journal of Geotechnical and Geoenvironmental Engineering. ASCE. January 2009. 14-25.

5. Senper, D. and Auvergne, G. A., 1982. Suction anchor piles- a proven alternative to driving or drilling. Offshore Technology Conference. Houston. USA. OTC 4206.

6. Tjeta, T.I., Guttormsen, T.R., Hermstad, J., 1986. Large-scale penetration test at a deepwatersite.Offshore Technology Conference, Houston, TX, Paper OTC 5103, 12pp.

7. Tran, M. N., Randolph, M. F. and Airey, D. W., 2004. Experimental study of suction installation of caissons in dense sand. Proceedings of the 23rd International Conference on Offshore Mechanics and Arctic Engineering, Vancouver, Canada, Paper number: OMAE04-51076.

8. Tran, M. N., Randolph, M. F., Airey, D. W., 2005. Study of Seepage Flow and Sand Plug Loosening in Installation of Suction Caissons in Sand. 15th International Offshore and Polar Engineering Conference, 19-24 June, 2005, Seoul, South Korea, 516-521.

9. Bye, A., Erbrich, C. T., Rognlien, B.,Tjelta, T. I., 1995. Geotechnical design of bucket foundations. Offshore Technology Conference, Houston, TX, Paper OTC 7793, 16pp.

10. Houlsby, G.T., Byrne, B.W., 2005. Design procedures for installation of suction caissons in sand. Proceedings of the Institution of Civil Engineers. Geotechnical Engineering, 158(3),135-144.

11. Tjelta, T.I., 1994.Geotechnical aspects of bucket foundations replacing piles for the Europipe 16/11-E Jacket. Offshore Technology Conference, Houston, TX, Paper OTC 7379, 10pp.

12. Tjelta, T.I., 1995. Geotechnical experience from the installation of the Europipe jacket with bucket foundations. Offshore Technology Conference, Houston, TX, Paper OTC 7795, 12pp.

13. Tran, M.N., Randolph, M.F., 2008. Variation of suction pressure during caisson installation in sand. Géotechnique, 58(1), 1-11.

14. Zhang, S., Zheng, Q., Liu, X., 2004.Finite element analysis of suction penetration seepage field of bucket foundation platform with application to offshore oilfield development. Ocean Engineering, 31, 1591-1599.

15. Tran, M.N., Randolph, M.F., Airey, D.W., 2007. Installation of suction caissons in sand with silt layers. Journal of Geotechnical and Geoenvironmental Engineering, 133(10), 1183-1191.

16. Ibsen, L.B., Thilsted, C.L., 2011. Numerical study of piping limits for suction installation of offshore skirted foundations and anchors in layered sand. Frontiers in Offshore Geotechnics II – Gouvernec& White (eds). Taylor & Francis Group, London, ISBN 978-0-415-58480-7

17. Harireche, O., Mehravar, M., Alani, A. M., 2013. Soil conditions and bounds to suction during the installation of caisson foundations in sand. Ocean Engineering (under review).

18. Bryant, W. R., Hottman, W., and Trabant, P. 1975. Permeability of unconsolidated and consolidated marine sediments, Gulf of Mexico. Marine Geotech., 1(1), 1-15.

19. Bennett, R. H., et al., 1990. In-situ porosity and permeability of selected carbonate sediment: Great Bahaman Bank. Part 1: measurements. Marine Geotech., 9(1), 1-28.

Figure Captions

Figure 1.

Normalised geometry and finite difference mesh

Figure 2.

Permeability profiles: Case A (constant permeability), case B (α = 0.288) and case C (α = 1.204)

Figure 3.

Normalised excess porewater pressure contours for scaled penetration depths h*=0.2, 1, 2.

a, c, e: constant permeability (case A); b, d, f: permeability with a high variability profile (case C, α = 1.204).

Figure 4.

Dimensionless pressure gradient as a function of scaled depth for different permeability profiles (cases A, B and C). a/ h* = 0.2; b/ h* = 1;c/ h* = 2.

Figure 5.

Reduction in the normalised lateral effective stress on caisson wall due to suction-induced seepage.a/ h* = 0.2; b/ h* = 1; c/ h* = 2.

Figure 6.

Effect of suction-induced seepage on soil resistance at caisson tip.

Figure 7.

Critical suction for piping on the inner caisson wall.a/ h* = 0.2; b/ h* = 1; c/ h* = 2.

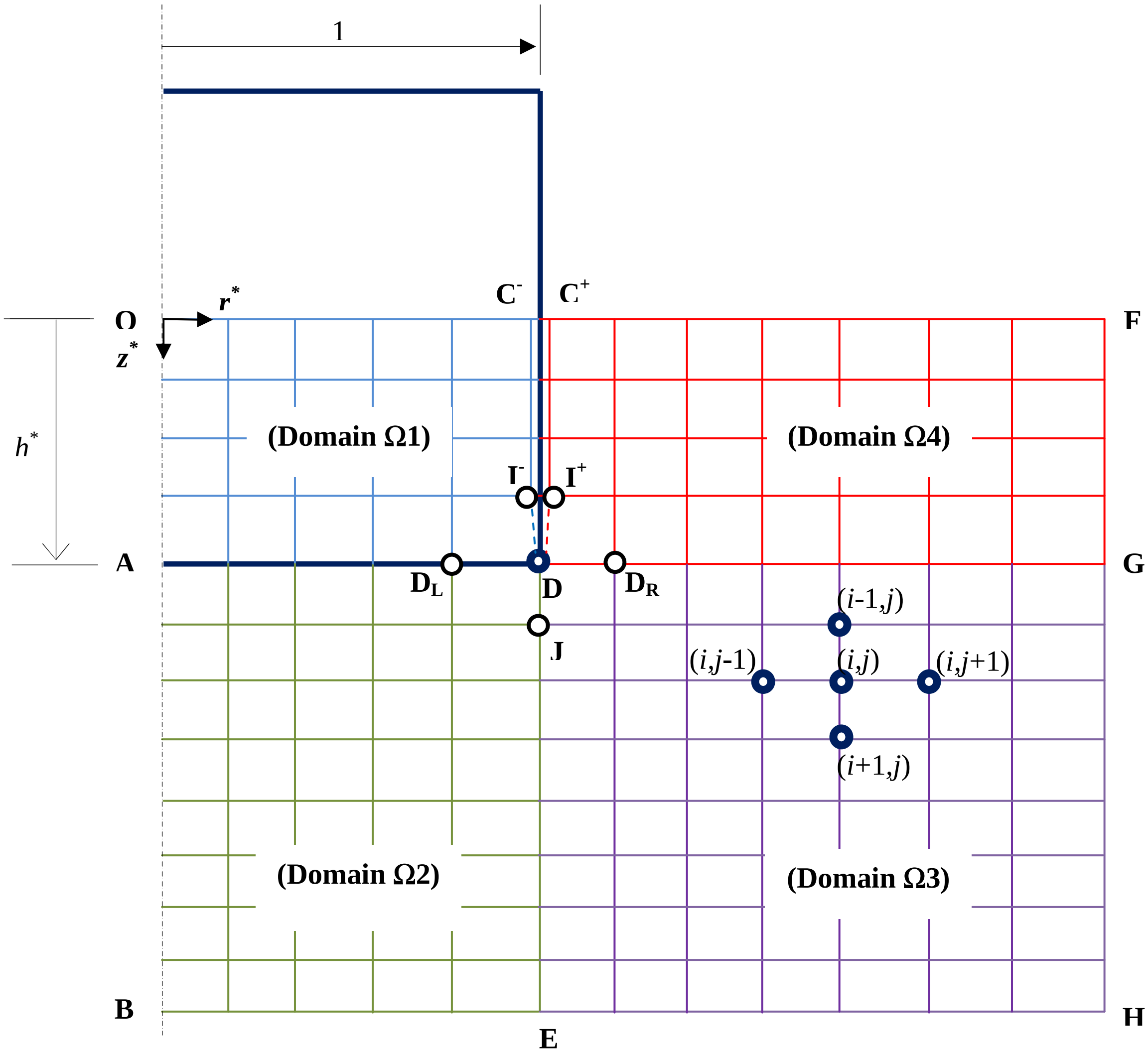

Figure 1.

(Colour on the Web)

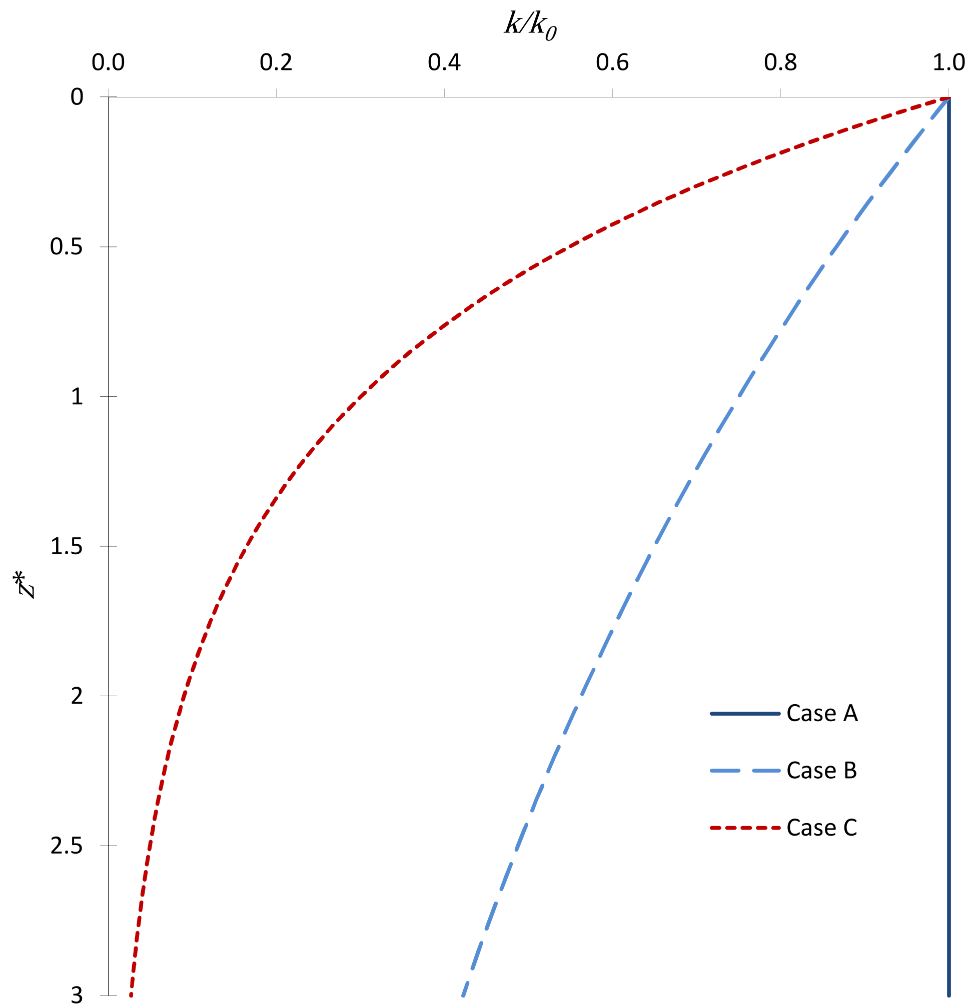

Figure 2.

(Colour on the Web)

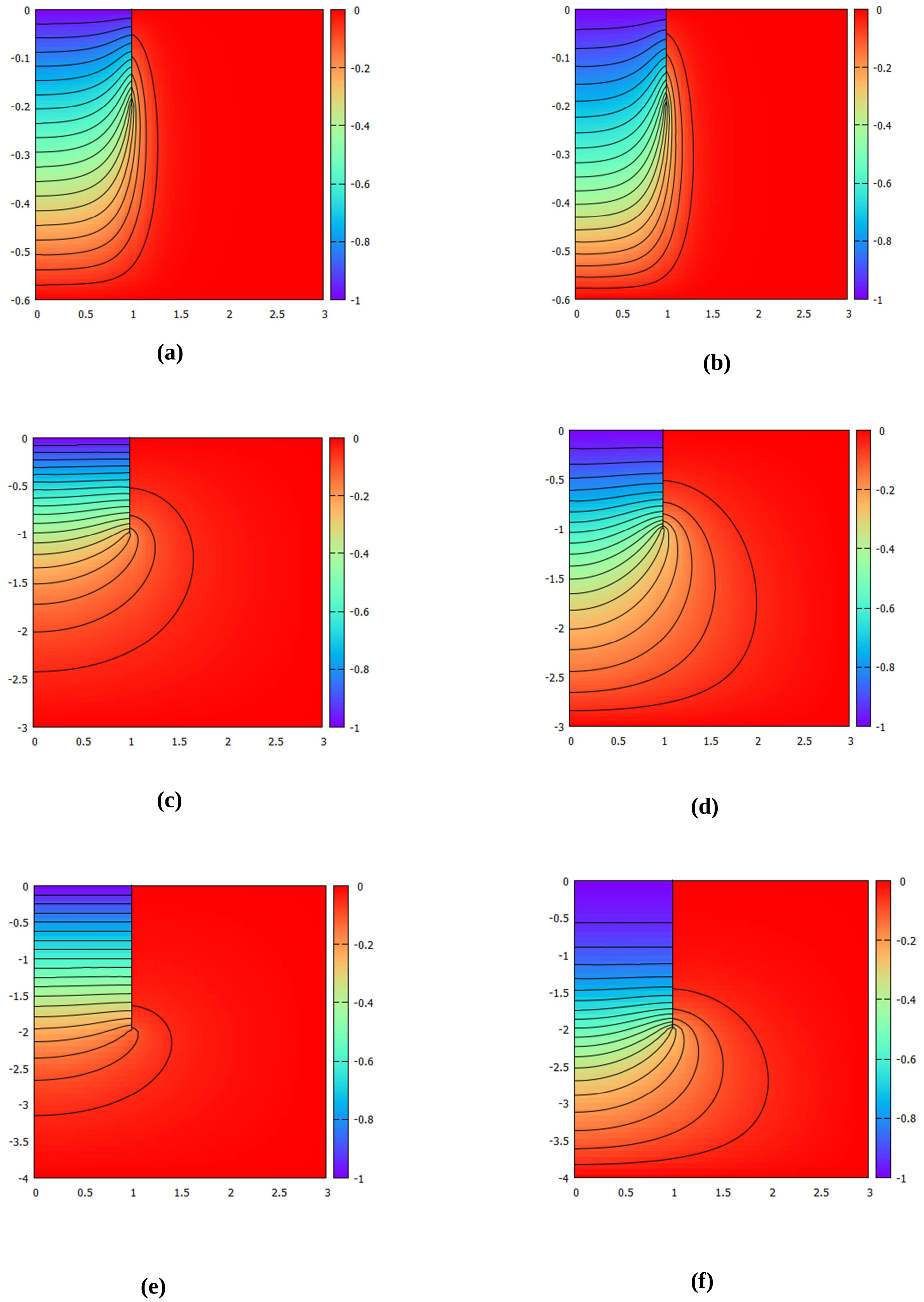

Figure 3.

(Colour on the Web)

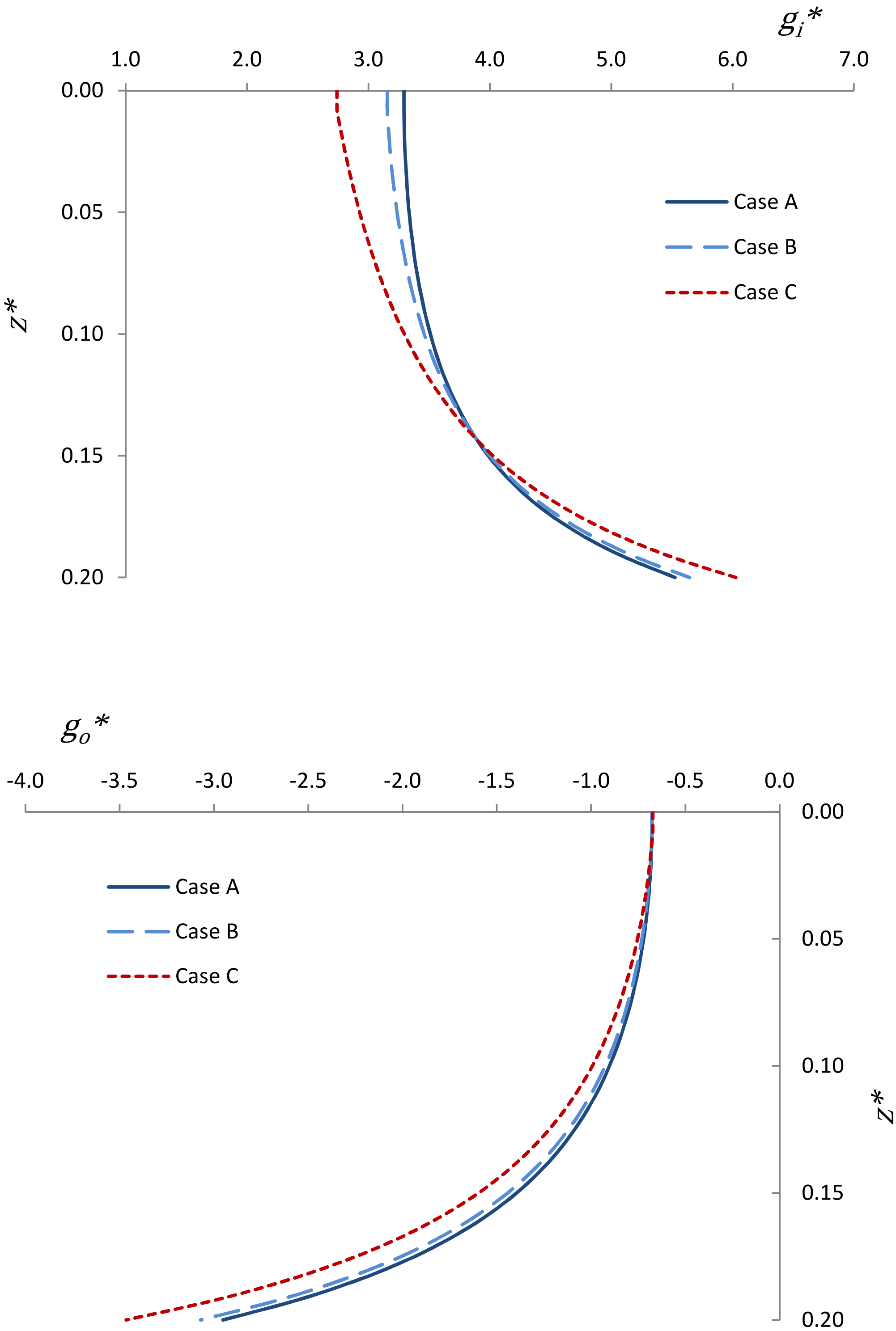

gi*
1.0
2.0
3.0
4.0
5.0
6.0
7.0
0.00
0.05
0.10
0.15
0.20
z*
Case A
Case B
Case C
go*
-4.0
-3.5
-3.0
-2.5
-2.0
-1.5
-1.0
-0.5
0.0
0.00
0.05
0.10
0.15
0.20
z*
Case A
Case B
Case C

(a)

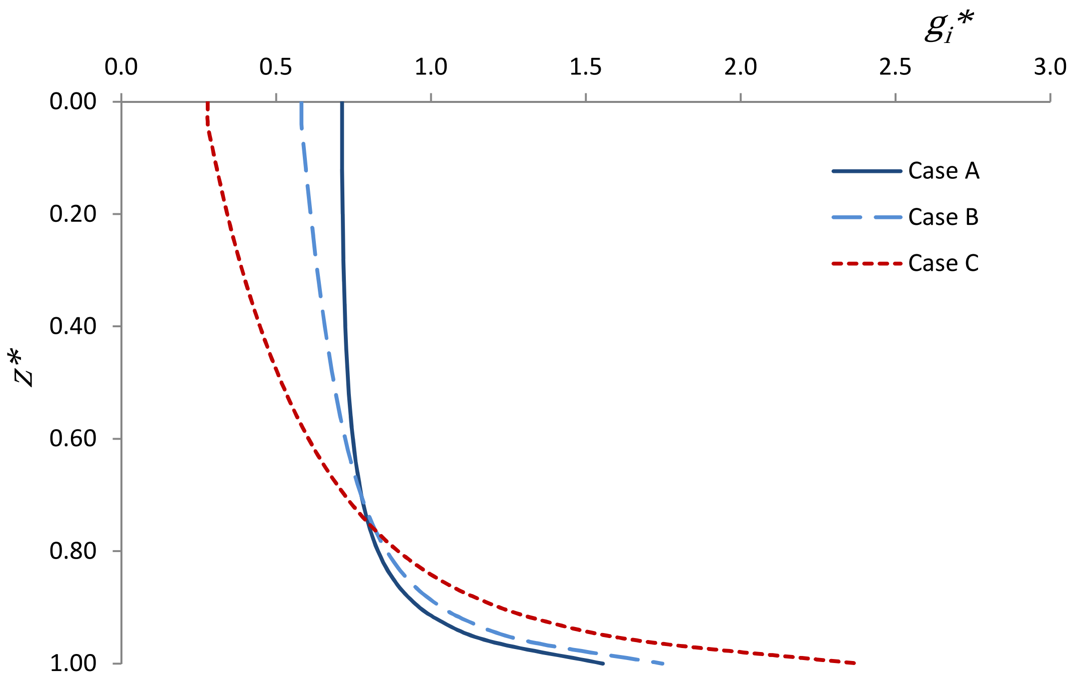

g_i*
0.0
0.5
1.0
1.5
2.0
2.5
3.0
0.00
0.20
0.40
0.60
0.80
1.00
z*
Case A
Case B
Case C

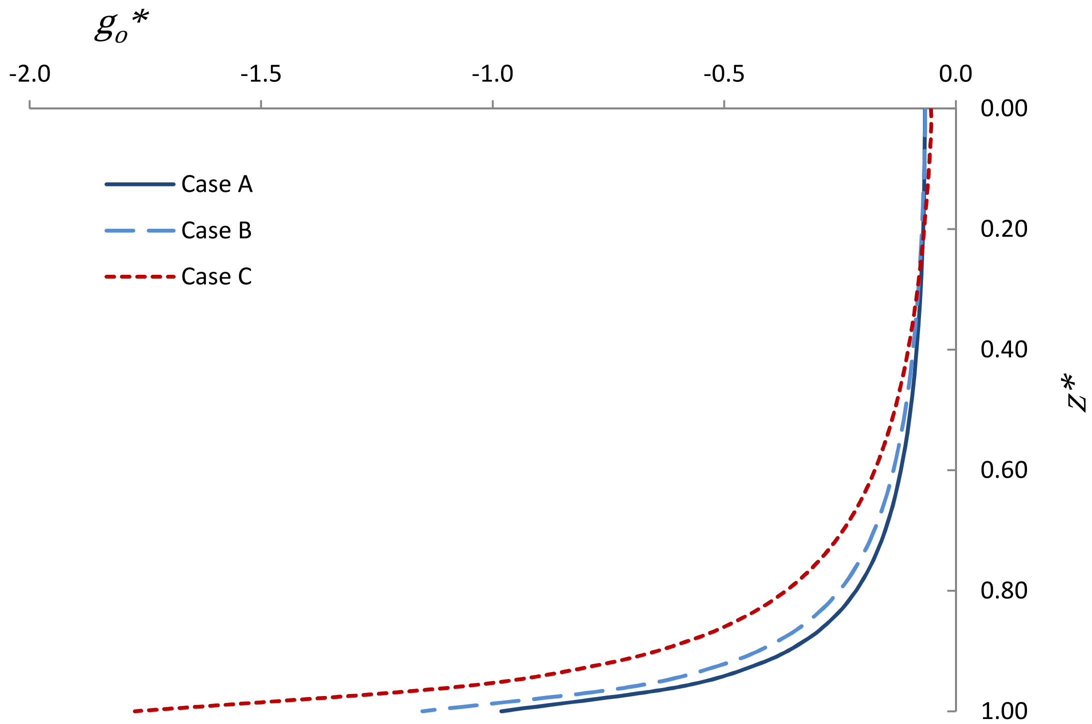

g_o*
-2.0
-1.5
-1.0
-0.5
0.0
0.00
0.20
0.40
0.60
0.80
1.00
z*
Case A
Case B
Case C

(b)

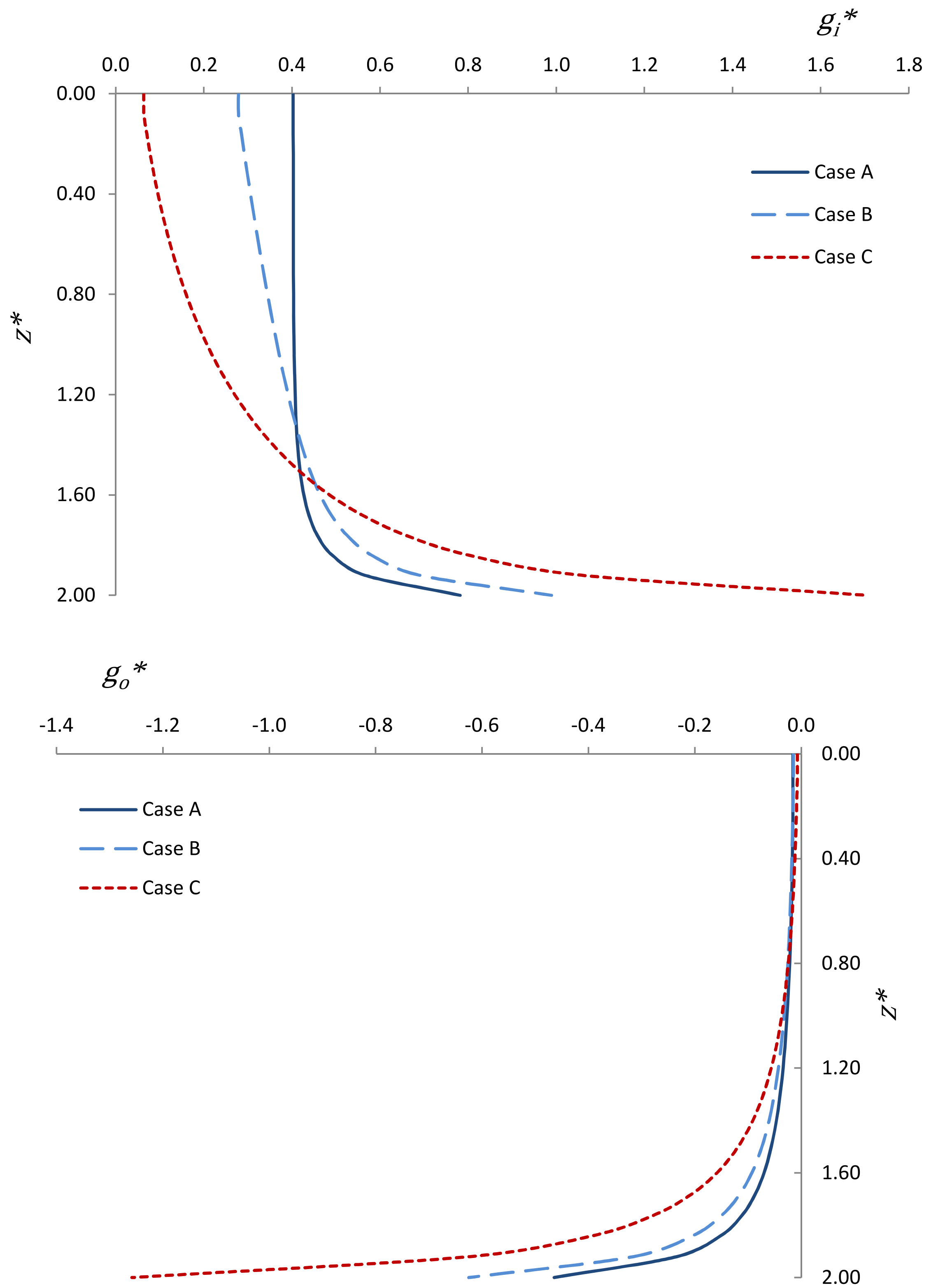

(c)

Figure 4.

(Colour on the web)

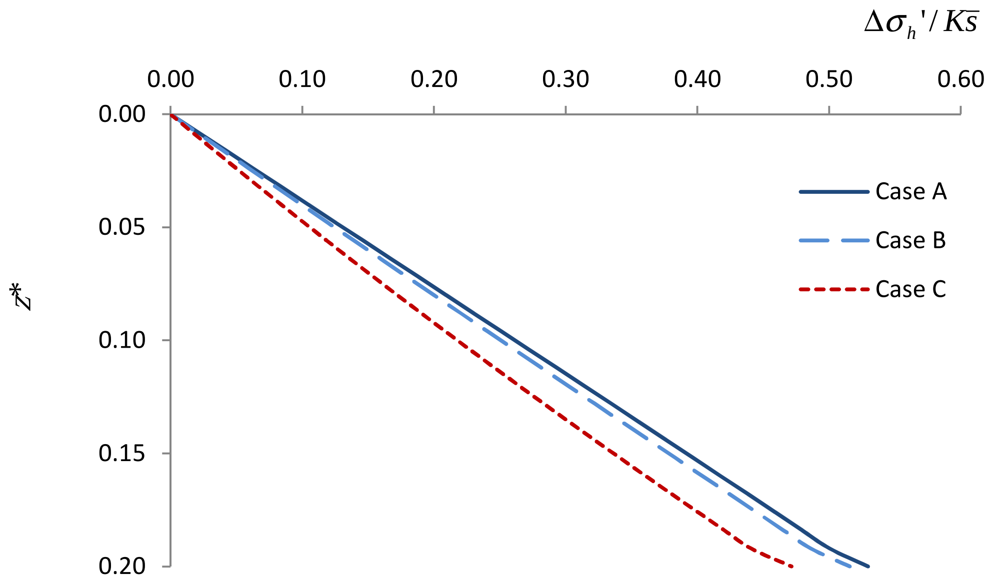
$\Delta\sigma_h'/K\overline{s}$
0.00
0.10
0.20
0.30
0.40
0.50
0.60
0.00
0.05
0.10
0.15
0.20
z^*
Case A
Case B
Case C

(a)

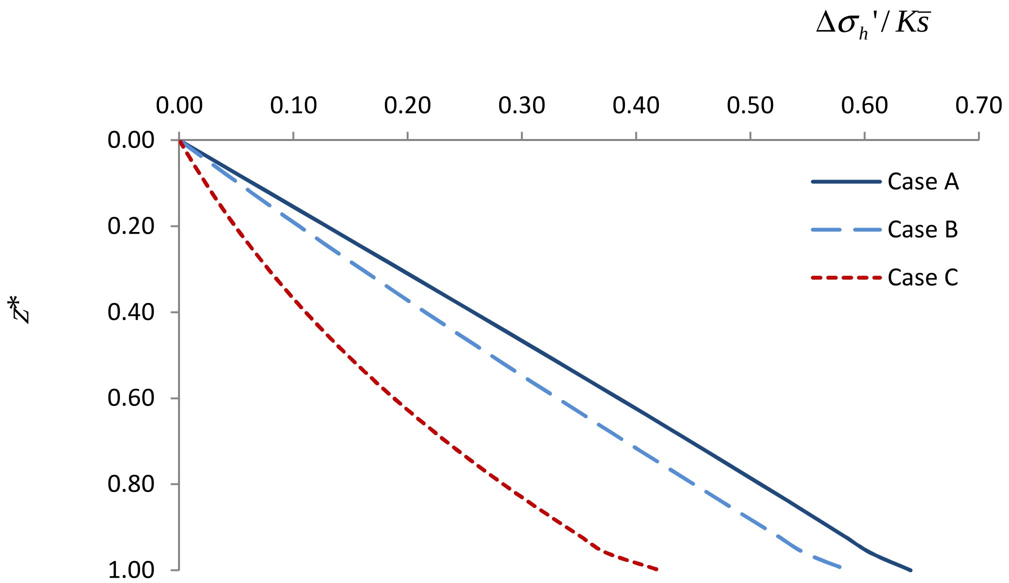
$\Delta\sigma_h'/K\overline{s}$
0.00
0.10
0.20
0.30
0.40
0.50
0.60
0.70
0.00
0.20
0.40
0.60
0.80
1.00
z^*
Case A
Case B
Case C

(b)

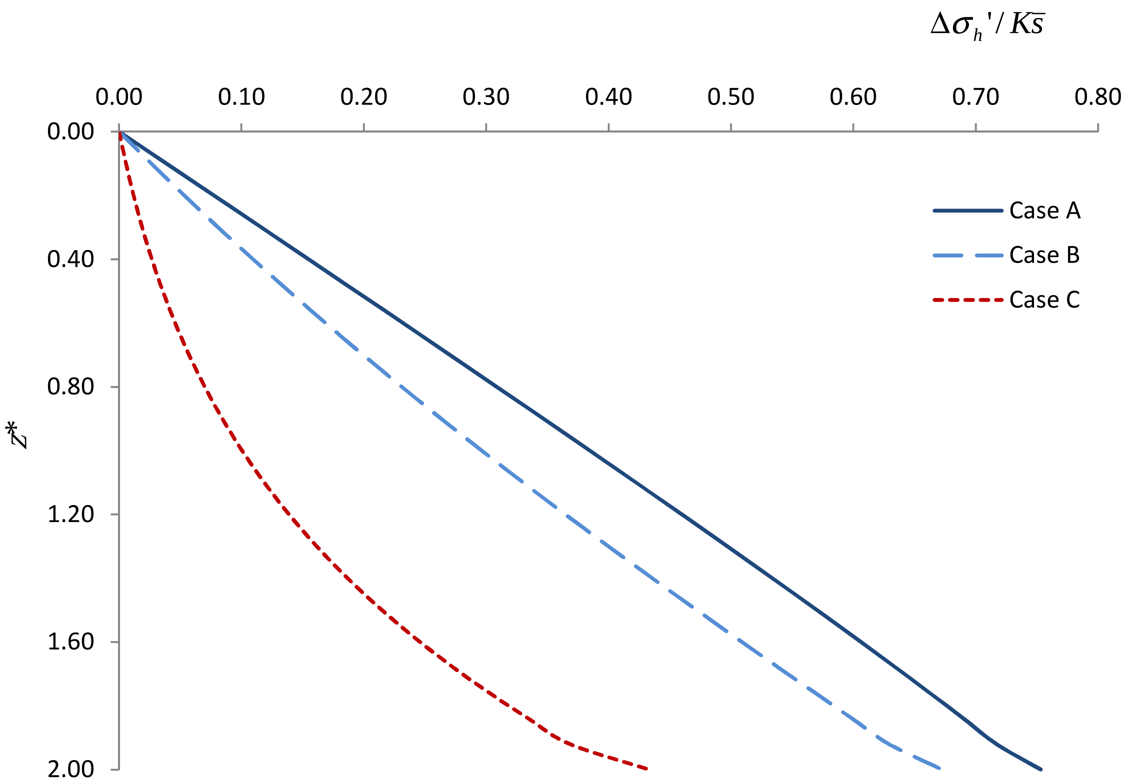

(c)

Figure 5.

(Colour on the web)

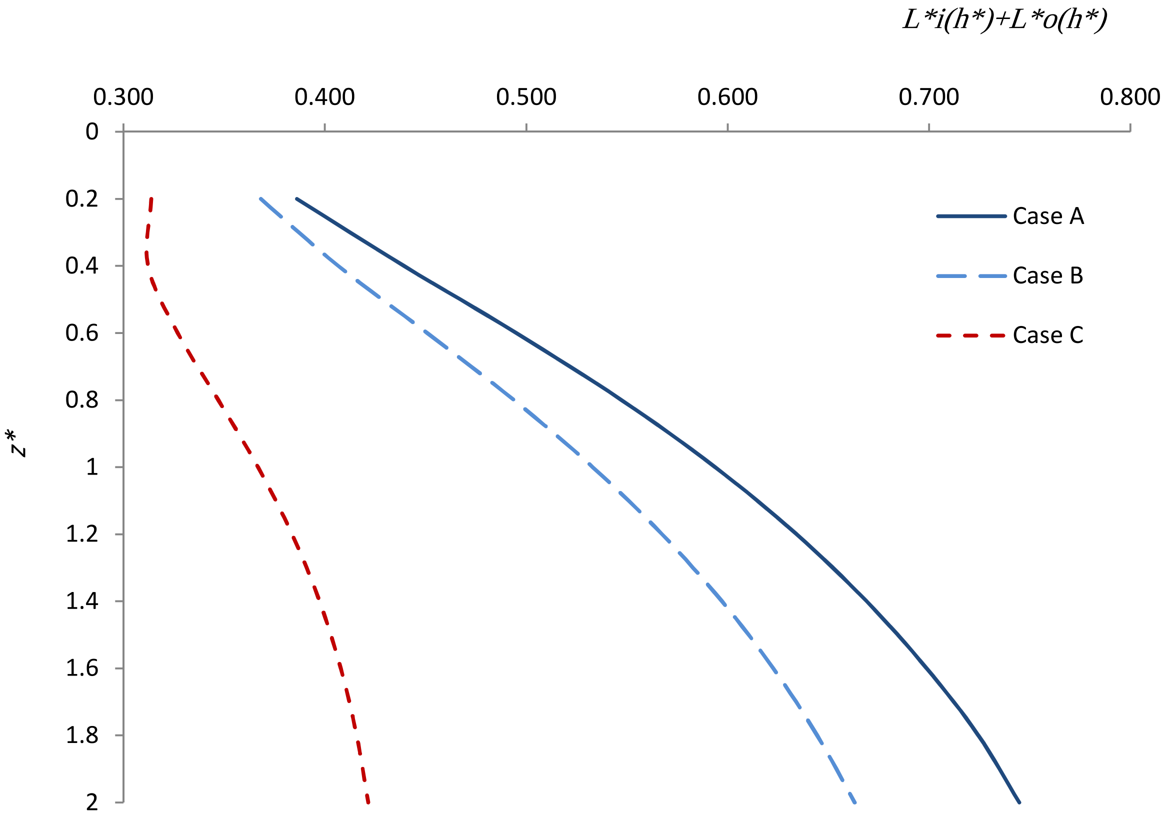

Figure 6.

(Colour on the web)

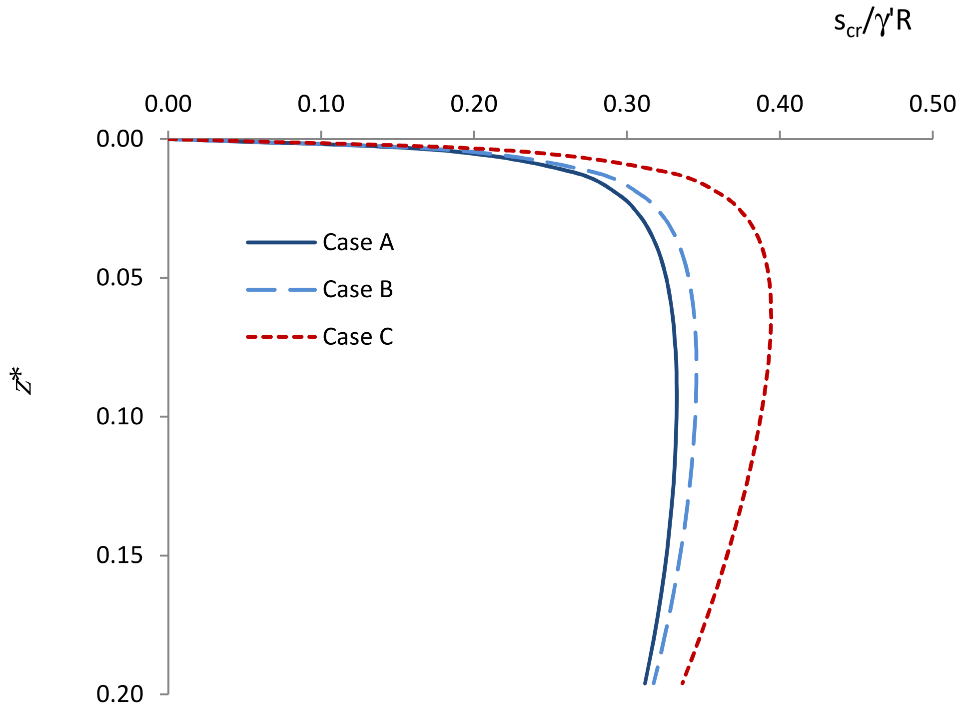
scr/γ'R
0.00
0.10
0.20
0.30
0.40
0.50
0.00
0.05
0.10
0.15
0.20
z*
Case A
Case B
Case C

(a)

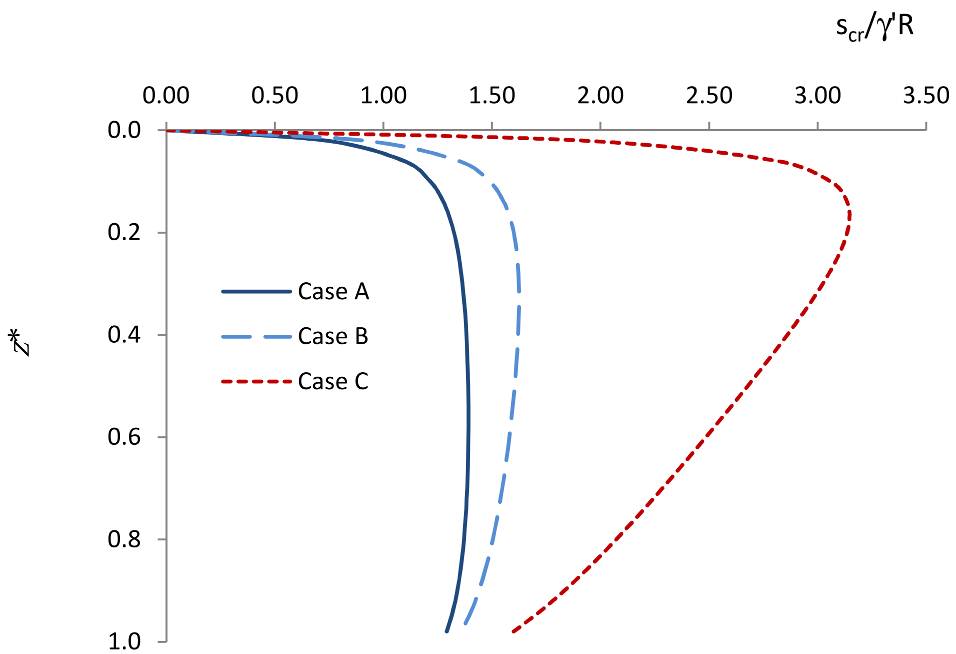
scr/γ'R
0.00
0.50
1.00
1.50
2.00
2.50
3.00
3.50
0.0
0.2
0.4
0.6
0.8
1.0
z*
Case A
Case B
Case C

(b)

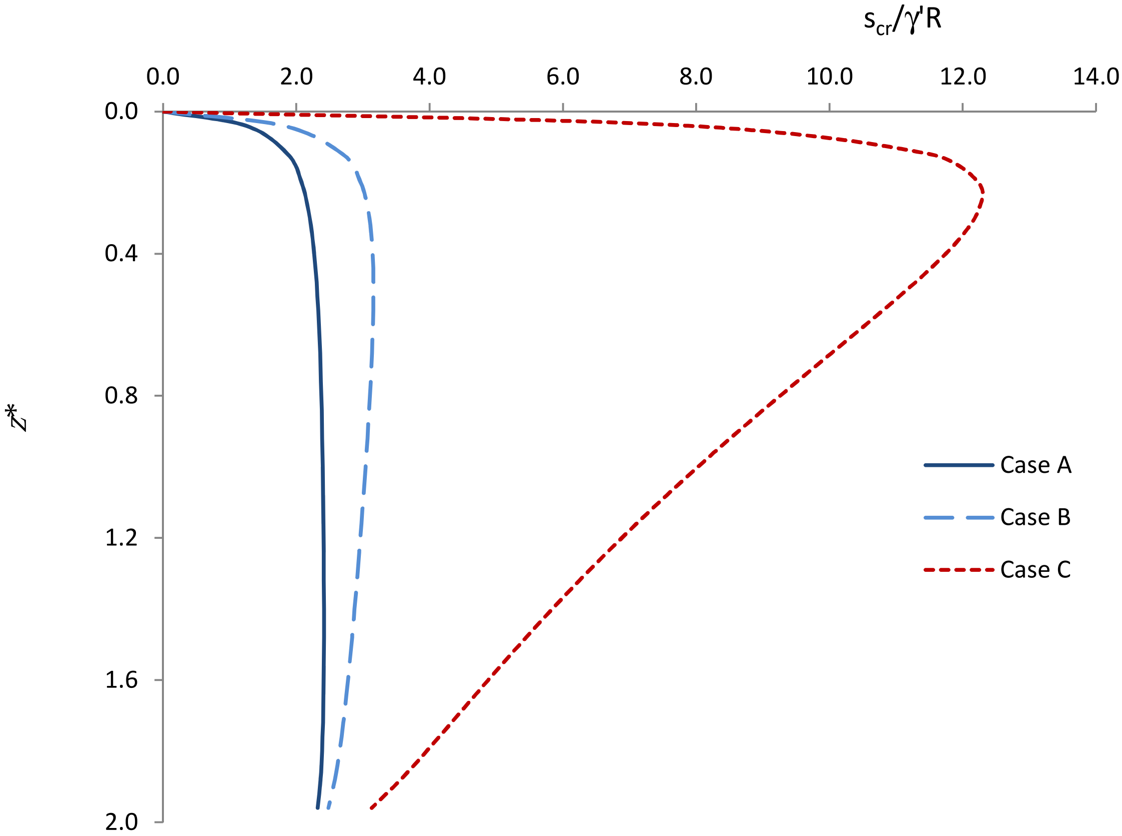

(c)

Figure 7.

(Colour on the web)